ELSEVIER

Physica D 132 (1999) 520–542

PHYSICA D

www.elsevier.com/locate/physd

A geometric model for coarsening during spiral-mode growth of thin films

T.P. Schulze *, R.V. Kohn

Courant Institute of Mathematical Sciences, New York University, 251 Mercer Street, New York, NY 10012, USA

Received 17 July 1998; accepted 15 March 1999
Communicated by H. Müller-Krumbhaar

Abstract

We study the coarsening observed in spiral-mode growth of thin films. The high-temperature superconductor $YBa_2Cu_3O_{7-\delta}$ provides a suitable model system. The density of spirals at the surface decreases as the film gets thicker. In other words, the grain size coarsens with distance from the substrate. We propose a simple mechanism for this coarsening, based on geometrical competition of spirals with different vertical growth rates. The consequences of this mechanism are developed both analytically and numerically in the limit where adatom attachment is controlled by surface diffusion. In particular, we show how the time-evolution of spiral density, film thickness, and surface roughness depend on the spiral growth rate statistics.

Keywords: Thin films; Spiral growth; Coarsening; YBCO

1. Introduction

The growth of epitaxial films has received a lot of attention (see [1] for a particularly relevant review article). Much is known about the mesoscopic consequences of layer-by-layer growth, in which new layers are created by the nucleation of islands on terraces. Less is known about the mesoscopic consequences of spiral growth, in which screw dislocations provide a continuous source of new steps. That is the topic of this paper.

The fundamentals of spiral growth were established by Burton, Cabrera and Frank [2]. At the heart of their model is a similarity solution for a single, steadily growing spiral. Their work has been extended by others, including Cabrera and Levine [3] and Müller-Krumbhaar et al. [4]. Monte Carlo simulations of spiral growth can be found in [5,6]. A Ginzburg–Landau simulation can be found in [7]. Karma and Plapp [8] use a phase-field approach to incorporate the effect of nonlocal diffusion. Most of this work has focused on the microscopic details of a single spiral or a few interacting spirals. Our focus, by contrast, is on the consequences of spiral growth for mesoscopic features such as grain size, surface roughness, and the overall growth rate.

* Corresponding author. E-mail: schulze@cims.nyu.edu.

0167-2789/99/$ – see front matter
PII: S0167-2789(99)00108-6

Our interest in spiral growth stems from its relevance to high-temperature superconducting (HTS) films. HTS films have been found to have higher critical currents and transition temperatures than the bulk state, making them superior for technological applications [9]. The material properties of the film are, at least in part, related to film microstructure. While our model is quite general, it is specifically motivated by the growth of $YBa_2Cu_3O_{7-\delta}$ (YBCO) films. This system exhibits a spiral growth morphology in parameter regimes that yield high-quality films, see e.g. [9,10]. These articles, and many others, feature scanning tunneling microscopy (STM) images of the YBCO film surface that show quite clearly the individual spirals. Each spiral consists of many terraces and ledges that wind around a central screw dislocation. The terrace widths are on the order of 10–100 nm while the step heights are one unit cell ($\sim$1 nm). YBCO films are commonly grown on MgO with c-axis orientation and a cube-on-cube epitaxy. There are small misalignments in the growth orientation where spirals meet to form low-angle grain boundaries. Occasionally, spirals will grow with more significant misalignment, e.g. rotated by 45° around the c-axis.

Each spiral determines a grain. The grain size is observed to coarsen as the YBCO film thickens, with 500 nm thick films exhibiting spiral widths at the surface which are on the order of 500 nm. Coarsening data can be found in [9–11], but coarsening has also been observed by many other authors, using various substrates and growth techniques. We know of three possible mechanisms that could drive this coarsening:

1. Yeadon et al. [10] propose that the screw dislocations are mobile. In their view coarsening is driven by elastic stress, which makes nearby dislocations of opposite sign migrate toward one another and eventually merge.
2. Ortiz et al. [12] propose that the valleys where spirals meet, i.e. the grain boundaries, have an associated 'defect energy'. In their view coarsening is driven by the tendency of the film to grow so as to decrease its defect energy.
3. We propose here that spatial heterogeneity leads naturally to coarsening. In our view, coarsening is a consequence of geometrical competition, whereby faster-growing grains overtake their slower-growing neighbors.

The purpose of this paper is to develop mechanism 3. We do not insist that it is the only coarsening mechanism operative in YBCO; all three mechanisms may actually be present. We nevertheless focus exclusively on mechanism 3, to gain a clear understanding of its consequences.

We shall use a simple geometric model to link heterogeneity to mesoscopic quantities such as surface roughness, the average growth rate, and the average grain size. The geometric character of our model is a simplification introduced to clarify the essential physics: we believe a more realistic treatment incorporating surface and bulk diffusion would have similar behavior. The key assumption of our model is that the (vertical) growth rate varies from spiral to spiral. This variation could be due, for example, to differences in the local structure at centers of the spirals. We do not attempt to model the origin or statistics of vertical growth rate variation; rather, we assume that it is given as constitutive information, and we explore its consequences.

Coarsening due to geometrical competition has been considered in other settings. Tang et al. [13] modeled the growth of an amorphous film by sputter deposition; there the mechanism of coarsening is self-shadowing, which gives large interfacial perturbations an advantage over their smaller neighbors. Thijssen et al. [14] modeled the growth of polycrystalline films made from crystals with few facets; there the mechanism of coarsening is competition between the faster-and slower-growing facets. Molchanov et al. [15] modeled the large-scale structure of the universe as a coarsening process in forced Burgers turbulence. Their work, though apparently unrelated to materials science, is in fact very closely connected to the present paper.

We introduce our geometric model in the following section, then discuss it more mathematically in Section 3. We mainly focus upon the case of diffusion-limited growth; in Section 4 we briefly discuss the implications of our analysis when this assumption is relaxed. Section 5 derives analytical results for coarsening and surface roughness based on this model; Section 6 verifies and extends these results using numerical simulation and Section 7 gives some concluding remarks.

We note in passing that the origin of the screw dislocations in YBCO c-axis films is not well understood. Some possible mechanisms are suggested in [10,16,17].

2. A geometric growth model

We begin by reviewing the physical mechanism of spiral growth, and the justification for a geometric model. A flux of atoms is raining down on the film surface. The deposition technique is not particularly relevant, but to fix ideas one can think of vapor deposition. The surface has many planar terraces and unit-cell high ledges. Atoms landing on the terraces move to the ledges by surface diffusion, where they attach themselves to the film.

We consider the case where there is no depletion of the diffusion boundary layers surrounding each ledge. This requires that the terrace width be much larger than the diffusion length $\sqrt{D\tau}$, where D is the surface diffusivity and τ is the typical adatom residence time. Under this condition of diffusion-limited growth, all the ledges see the same local adatom concentration, so one expects the normal velocity U to be a constant to leading order. We shall ignore corrections due to curvature, but we include the effect of crystalline anisotropy by allowing the normal velocity to be a function of growth direction: $U = U(\hat{\boldsymbol{n}})$, where $\hat{\boldsymbol{n}}$ is a unit vector in the direction of *horizontal* growth.

An interesting generalization of this setting would let the ledge velocity U depend on the terrace width, i.e. the distance between ledges. Such dependence would provide a geometrical (albeit oversimplified) model of growth beyond the diffusion-limited regime. Unfortunately, as we explain in Section 4, our method for predicting the coarsening and other mean film properties does not extend to this case. We therefore restrict our attention to $U = U(\hat{\boldsymbol{n}})$.

Under this simple motion law, an initial landscape of ledges grows horizontally (in planes parallel to the substrate); each ledge continues growing until it is blocked by another ledge or it reaches the boundary of the film. In spiral growth there is no nucleation on terraces. Instead, screw dislocations provide a continuous source of new ledges. The spiral associated with a screw dislocation looks like a driveway winding its way up a mountain (Fig. 1(a)). The spiral ends precipitously at the top, so there is always an edge for the growth of a new layer of atoms. The theories for steady-state spirals (references given above) have the spiral terminating with a finite radius of curvature so that ledge growth at the top of the spiral causes it to precess. The spiral endpoint can either remain fixed or travel in a circle, depending on the details of the theory.

For our purposes, this detailed picture of the spiral is unnecessary. The essential point is the existence of a continuous source of new growth layers at the spiral center. Taking a somewhat more macroscopic point of view we can say that the spiral grows by repeatedly nucleating new growth layers at the screw dislocation, which then grow outward with uniform speed U. The resulting picture is rather like that of island growth: it produces a wedding cake rather than a spiral driveway (compare Figs. 1(a,b)). There are some differences, of course, from true island growth: our nucleation of new growth layers occurs at precisely the same point from one layer to the next and we envision a nucleation rate which varies from spiral to spiral – the idea being that variation in local structure produces different precession rates for different spirals.

The screw dislocations are formed very early in the YBCO-film growth process. We shall assume that these dislocations are distributed randomly on the substrate, at points $\boldsymbol{x}_j$. We further assume that the jth dislocation remains at a fixed position, and produces vertical growth at a constant rate v_j until it is covered by the spiral associated with another dislocation. Our analytical results assume that no new dislocations are formed after the deposition process begins, though we explore the effect of relaxing this assumption in a simulation. We use a Poisson point process (PPP) to generate the screw dislocations, so the expected number of screws in a given region is proportional to its area. We suppose the vertical growth rates v_j are drawn independently from some statistical distribution, forming what is known as a *marked* PPP.

Since our interest is in mesoscopic quantities, we neither need nor want to resolve the individual steps and terraces. Therefore we work in the continuum limit obtained by letting the step height and terrace width tend to zero while keeping their ratio (the slope of the spiral) fixed. In this limit our wedding-cake structures become cones (Fig. 1(c)),

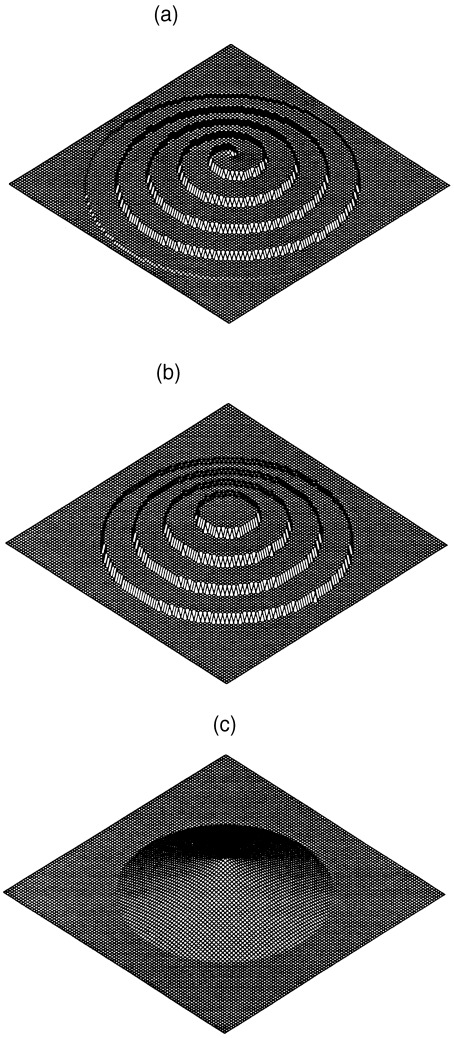

Fig. 1. The relationship between (a) a detailed picture of the spiral growth process, (b) an intermediate model that mimics spiral growth via nucleation at the top of a wedding cake, and (c) the continuum limit in which the wedding cake becomes a cone.

and the ledges become level sets of the surface height function. The growth produced by adatom attachment is directed normal to this level set, in the plane parallel to the substrate.

To understand the essential issues, it is helpful to visualize the one-dimensional version of this problem. Figure 2(a) shows the profile produced by five screw dislocations at a certain time (solid lines) and a slightly later time (dotted lines), when the vertical velocities $v_2 = v_3$ are larger than $v_1 = v_4 = v_5$ and the horizontal velocity is 1. The jth screw is associated with a growing peak of constant slope v_j and increasing height $v_j t$ (grey lines). This peak is the growth profile associated with a single, isolated screw dislocation at x_j. Our model says that the film's growth profile is the envelope of these peaks. The valley where two peaks meet represents a grain boundary. In the setting of Fig. 2(a), the grain boundaries move relative to the substrate as time evolves, because $v_2 = v_3$ is larger than $v_1 = v_4 = v_5$. Eventually the sources at x_1, x_4, and x_5 are covered by the peaks associated with x_2 and x_3 (in Fig. 2(b) the source at x_1 has been covered). As time proceeds, an increasingly large percentage of the film is occupied by the grains associated with the faster-growing spirals. This simple example shows how a distribution of

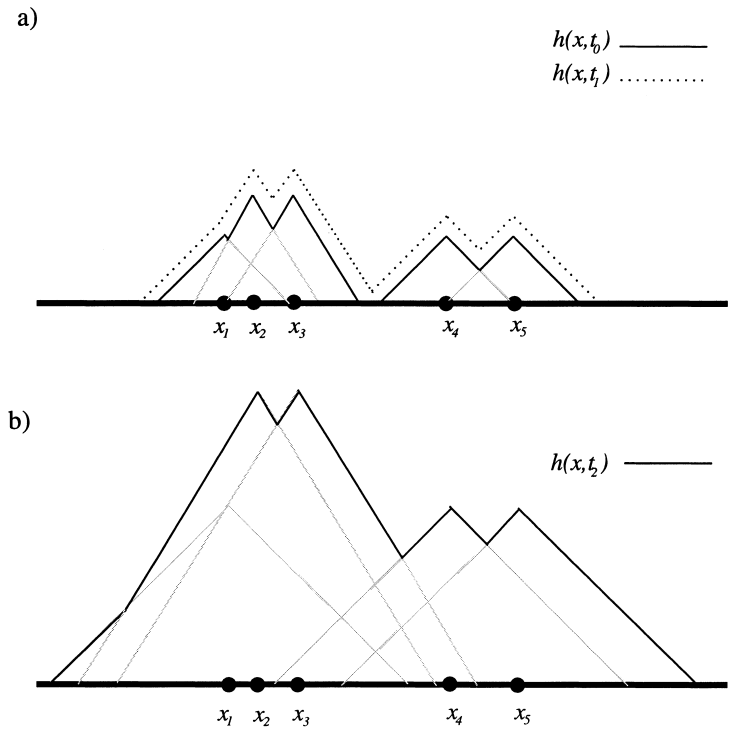

Fig. 2. (a) The profile produced by five screw dislocations at a certain time (solid lines) and a slightly later time (dashed lines), when the vertical velocities $v_2 = v_3$ are larger than $v_1 = v_4 = v_5$. The peaks meet at grain boundaries, which move (relative to the substrate) as the film evolves. (b) The profile of the film after the source at x_1 has been covered. As time proceeds, an increasingly large percentage of the film is occupied by the fast-growing grains.

growth rates leads to coarsening. The two-dimensional picture is similar: the film surface is an evolving collection of cones, centered at points $\boldsymbol{x}_j$ with vertical velocity v_j; the valleys where the cones meet are the grain boundaries.

3. Evolution of the film surface, Huygens' principle and a solution formula

Our goal is an analysis of the mesoscopic features of growth – particularly the time dependence of average thickness, surface roughness, and grain size. Our principal tool in the pursuit of this goal is an explicit solution formula for the thickness of the film:

$$h(\boldsymbol{x}, t) = \max_j \{v_j[t - T(\boldsymbol{x}_j, \boldsymbol{x})], 0\}. \tag{1}$$

Here $h(\boldsymbol{x}, t)$ is the height of the film above the substrate at position $\boldsymbol{x} \in \boldsymbol{R}^2$ and time $t > 0$; $\boldsymbol{x}_j$ is the position of the jth screw dislocation (source); $v_j > 0$ is the vertical growth rate of the jth source; and $T(\boldsymbol{x}_j, \boldsymbol{x})$ is the time it takes a ledge to advance from $\boldsymbol{x}_j$ to $\boldsymbol{x}$. The expression for the travel time $T(\boldsymbol{x}_j, \boldsymbol{x})$ is discussed below (Section 3.3, see especially Eq. (14)). For the isotropic case, we take $U(\hat{\boldsymbol{n}}) \equiv 1$, so that the ledges move at unit speed in all directions. Huygens' principle then gives $T(\boldsymbol{x}_j, \boldsymbol{x}) = |\boldsymbol{x}_j - \boldsymbol{x}|$ and the solution formula (1) reduces to

$$h(\boldsymbol{x}, t) = \max_j \{v_j[t - |\boldsymbol{x}_j - \boldsymbol{x}|], 0\}. \tag{2}$$

Our justification of Eqs. (1) and (2) will combine well-known facts about interface motion with arguments from the recent work of Molchanov et al. [15]. Our analysis requires the speed function $U(\hat{\boldsymbol{n}}) > 0$ to be a *convex* velocity in the sense that its homogeneous extension of degree one,

$$U_{\mathrm{e}}(\boldsymbol{x}) \equiv |\boldsymbol{x}| U\left(\frac{\boldsymbol{x}}{|\boldsymbol{x}|}\right), \tag{3}$$

is a convex function of $\boldsymbol{x} \in \boldsymbol{R}^2$. This clearly holds in the isotropic case, and more generally when the anisotropy is sufficiently weak. Convexity is required for the existence of an anisotropic Huygens' principle (see Section 3.2). Our problem makes physical and mathematical sense for a nonconvex ledge velocity, but we doubt the existence of a solution formula like Eq. (1) in that case.

Sections 3.1–3.5 are somewhat mathematical. A reader who is content to accept Eq. (1) as a formula for the surface height can skip directly to Section 5 for the discussion of its consequences.

3.1. The evolution equation

We have thus far specified the solution (1), but not the equation it satisfies. An evolution equation for the film thickness $h(\boldsymbol{x}, t)$ follows from the fact that the total time derivative of h along a given level set $h = c$ is zero:

$$h_t + \boldsymbol{u} \cdot \boldsymbol{\nabla} h = 0. \tag{4}$$

The velocity and gradient indicated in this equation are vectors in the plane of the level set; growth in the vertical direction is generated only at the screw dislocations and is discussed below. If we combine this equation with our anisotropic growth law

$$\boldsymbol{u} \cdot \hat{\boldsymbol{n}} = U(\hat{\boldsymbol{n}}),$$

using the expression for the outward normal to the level sets

$$\hat{\boldsymbol{n}} = -\frac{\boldsymbol{\nabla} h}{|\boldsymbol{\nabla} h|},$$

we can write Eq. (4) in the form of a Hamilton–Jacobi equation:

$$h_t = U(\hat{\boldsymbol{n}})|\boldsymbol{\nabla} h|. \tag{5}$$

In the isotropic case this reduces to $h_t = |\boldsymbol{\nabla} h|$; in the one-dimensional setting of Fig. 2 it becomes $h_t = |h_x|$.

The preceding argument is well-known. It lies at the foundation of the *level set method* for analyzing and computing interface motion, see e.g. [18,19]. It can be linked to the earlier viewpoint of [20] based on the method of characteristics, see [21]. Some care is required, however, concerning what we mean by a 'solution' of Eq. (5). It is not enough to say that the equation holds wherever h is smooth; to determine h uniquely we must also say what happens at the valleys (grain boundaries) and peaks (screw dislocations), where h is not smooth. This issue is closely related to the theory of 'viscosity solutions' of Hamilton–Jacobi equations (see e.g. [22]). However, the viscosity solution of Eq. (5) is not what we want: it takes no account of the sources $\boldsymbol{x}_j$ and growth rates v_j. In fact, the viscosity solution is incapable of rising above the maximum height of its initial data:

$$h(\boldsymbol{x}, t) \leq \max_{\boldsymbol{x} \in \boldsymbol{R}^2} h(\boldsymbol{x}, 0),$$

and solutions develop plateaus rather than peaks (Fig. 3).

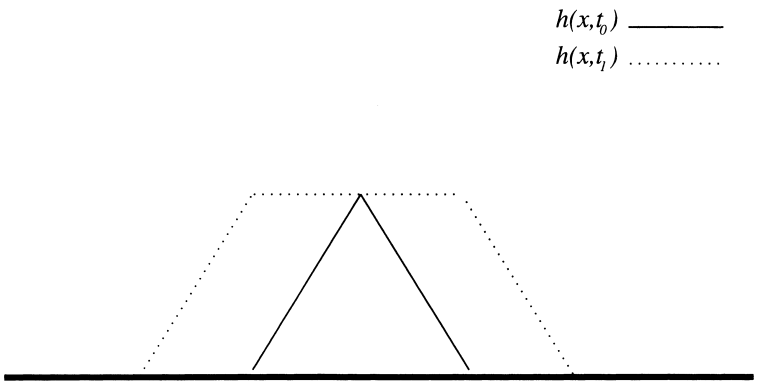

Fig. 3. Schematic illustration of the maximum principal for viscosity solutions of Eq. (5). Cone-shaped initial data will develop a plateau rather than a peak.

The recent work of Molchanov et al. [15] gives a way of addressing this issue. Informally, one can consider the viscosity solution of

$$h_t = U(\hat{\boldsymbol{n}})|\nabla h| + \sum_j v_j I(\boldsymbol{x} - \boldsymbol{x}_j) \tag{6}$$

where

$$I(\boldsymbol{x} - \boldsymbol{x}_j) = \begin{cases} 1 & \text{for} \quad \boldsymbol{x} = \boldsymbol{x}_j \\ 0 & \text{otherwise.} \end{cases}$$

This does not strictly make sense, because the right hand side is too singular for the theory of viscosity solutions to apply. One should approximate the function $I(\boldsymbol{x} - \boldsymbol{x}_j)$ by something smoother, solve the evolution equation, then pass to the limit (6). The evolution equation requires an initial condition. Our solution formula (1) corresponds to

$$h(\boldsymbol{x}, 0) = 0.$$

One can show by arguing as in [15] that the solution of Eq. (6) with this initial condition is the same as the one defined in Section 3.2 by a variational principle.

3.2. Variational formulation

The link between Hamilton–Jacobi equations and optimal control theory is known. This link provides the connection between Eq. (6) and the solution formula (1). It also provides an anisotropic version of Huygens' principle and explains why our analysis is restricted to convex velocity functions $U(\hat{\boldsymbol{n}})$. Finally, it gives a triangle inequality for travel times Eq. (15), which we shall need in Section 3.4.

To explain this link, consider the general problem of maximizing

$$S[\boldsymbol{r}(s)] = \int_0^t [\Phi(\boldsymbol{r}) - g(\dot{\boldsymbol{r}})]\,\mathrm{d}s$$

over the set of paths $P = \{\boldsymbol{r}(s) : [0, t] \to \boldsymbol{R}^2, \boldsymbol{r}(t) = \boldsymbol{x}\}$ that start at an arbitrary location and end at $\boldsymbol{x}$ in time t. Let $h(\boldsymbol{x}, t)$ be the optimal value:

$$h(\boldsymbol{x}, t) = \max_P S[\boldsymbol{r}(t)]. \tag{7}$$

It is known (see e.g. [22]) that $h(\boldsymbol{x}, t)$ is the viscosity solution of the differential equation

$$h_t = \Phi + g^*(-\boldsymbol{\nabla} h) \tag{8}$$

with initial value $h(\boldsymbol{x}, 0) = 0$. Here g^* is the Fenchel transform of g:

$$g^*(\boldsymbol{x}) = \max_{\boldsymbol{y}} [\boldsymbol{y} \cdot \boldsymbol{x} - g(\boldsymbol{y})]. \tag{9}$$

(See e.g. [23] for a convenient summary of results about the Fenchel transform.)

To see informally why Eq. (7) satisfies Eq. (8), look at the variational problem defining $h(\boldsymbol{x}, t + \delta t)$. It is natural to consider the trial path which follows the optimal path in the definition of $h(\boldsymbol{x} - \delta \boldsymbol{x}, t)$, then continues in a straight segment for time δt to end at $\boldsymbol{x}$. The best path for the definition of $h(\boldsymbol{x}, t + \delta t)$ is obtained by optimization over $\delta \boldsymbol{x}$. In the limit $\delta t \to 0$ this gives

$$h(\boldsymbol{x}, t + \delta t) = \max_{\delta \boldsymbol{x}} \left\{ h(\boldsymbol{x} - \delta \boldsymbol{x}, t) + \left[\Phi(\boldsymbol{x}) - g\left(\frac{\delta \boldsymbol{x}}{\delta t} \right) \right] \delta t \right\}.$$

Expanding $h(\boldsymbol{x} - \delta \boldsymbol{x}, t)$ in a Taylor series about $\boldsymbol{x}$ gives

$$\frac{h(\boldsymbol{x}, t + \delta t) - h(\boldsymbol{x}, t)}{\delta t} = \Phi(\boldsymbol{x}) + \max_{\delta \boldsymbol{x}/\delta t} \left[-\frac{\delta \boldsymbol{x}}{\delta t} \boldsymbol{\nabla} h(\boldsymbol{x}, t) - g\left(\frac{\delta \boldsymbol{x}}{\delta t} \right) \right],$$

which is equivalent to Eq. (8) as $\delta t \to 0$.

To make Eq. (8) agree with our differential equation (6) we have only to make appropriate choices of Φ and g. We evidently want

$$\Phi(\boldsymbol{x}) = \sum_j v_j I(\boldsymbol{x} - \boldsymbol{x}_j), \tag{10}$$

and

$$g^*(\boldsymbol{\nabla} h) = |\boldsymbol{\nabla} h| U\left(\frac{\boldsymbol{\nabla} h}{|\boldsymbol{\nabla} h|} \right) = U_{\mathrm{e}}(\boldsymbol{\nabla} h). \tag{11}$$

The second condition requires U_{e} to be convex, since g^* – being the maximum of linear functions by Eq. (9) – is convex for any g. If U_{e} is convex, then we may take g to be the Fenchel transform of U_{e}. Since U_{e} has linear growth at ∞, its Fenchel transform takes only the values 0 and ∞, i.e. it is the *indicator* function of a convex set W:

$$g(\boldsymbol{x}) = U_{\mathrm{e}}^*(\boldsymbol{x}) = \begin{cases} 0 & \text{if} \quad \boldsymbol{x} \in W \\ \infty & \text{if} \quad \boldsymbol{x} \notin W. \end{cases}$$

The set W is known as the Wulff shape associated with $U(\hat{\boldsymbol{n}})$; its analytical expression is

$$W = \left\{ \boldsymbol{x} : |\boldsymbol{x}| \leq w\left(\frac{\boldsymbol{x}}{|\boldsymbol{x}|} \right) \right\},$$

where for any unit vector $\hat{\boldsymbol{r}}$

$$w(\hat{\boldsymbol{r}}) = \min_{\hat{\boldsymbol{n}} \cdot \hat{\boldsymbol{r}} > 0} \left[\frac{U(\hat{\boldsymbol{n}})}{\hat{\boldsymbol{n}} \cdot \hat{\boldsymbol{r}}} \right]. \tag{12}$$

There is a well-known geometrical construction of the Wulff shape W: it is formed by making a polar plot of the speed function $U(\hat{\boldsymbol{n}})$, constructing lines which are orthogonal to the radius vector at each point on this plot, and taking the inner envelope of those lines.

The Wulff construction also arises in the analysis of anisotropic surface energy. If the surface energy density is $\gamma(\hat{\boldsymbol{n}})$ then the associated Wulff shape, defined as above with U replaced by γ, has minimal surface energy for given volume. We emphasize, however, that our model omits any effect of surface energy. Therefore the relevant Wulff shape is the kinetic one, associated with the growth velocity $U(\hat{\boldsymbol{n}})$.

3.3. Travel time and the solution formula

It remains to link our differential equation (6) with our solution formula (1). The key, of course, is the variational principle (7). Using the choices Eqs. (10) and (11) it becomes

$$h(\boldsymbol{x},t) = \max_{\dot{\boldsymbol{r}}\in W, \boldsymbol{r}(t)=x} \int_0^t \sum_j v_j I(\boldsymbol{x}-\boldsymbol{x}_j)\,\mathrm{d}s,$$

which can be written more simply as

$$h(\boldsymbol{x},t) = \max_{\text{admissible paths}} \sum_j v_j \times (\text{residence time at } \boldsymbol{x}_j). \tag{13}$$

We like to visualize this optimization as follows. For any admissible path $\boldsymbol{r}(s)$ in the substrate plane (defined for $0 \le s \le t$, with speed $\dot{\boldsymbol{r}}(s) \in W$ and endpoint $\boldsymbol{r}(t) = \boldsymbol{x}$), consider the path in physical space with the same planar projection, which starts at height 0 and accumulates height at rate v_j during any interval when $\boldsymbol{r}(s)$ remains at a dislocation site $\boldsymbol{x}_j$ (Fig. 4(a)). The sum on the right hand side of Eq. (13) is the height of this physical space path at time t.

A useful observation concerning Eq. (13) is the fact that

$$\text{residence time at dislocation sites} = t - \text{travel time}.$$

It follows that the optimal path must be efficient: it minimizes travel time.

We claim that paths which minimize travel time (among all paths with the same endpoints, and velocity in W) are necessarily straight paths with constant velocity. Indeed, consider any path $\boldsymbol{r}(s)$, straight or not, traveling from $\boldsymbol{x}_a$ to $\boldsymbol{x}_b$ in minimal time T:

$$\boldsymbol{r}(0) = \boldsymbol{x}_a, \qquad \boldsymbol{r}(T) = \boldsymbol{x}_b, \qquad \dot{\boldsymbol{r}}(s) \in W.$$

Its average velocity must belong to W, since W is convex. The average velocity is evidently

$$\bar{\boldsymbol{u}} = \frac{1}{T}\int_0^T \dot{\boldsymbol{r}}(t)\,\mathrm{d}t = \frac{\boldsymbol{x}_b - \boldsymbol{x}_a}{T}.$$

Therefore the straight path $\rho(s) = \boldsymbol{x}_a + \bar{\boldsymbol{u}}s$ is admissible, and it too arrives at $\boldsymbol{x}_b$ at time T. If the original path $\boldsymbol{r}(s)$ did not have constant velocity then $\bar{\boldsymbol{u}}$ would be in the interior of W (assuming W is strictly convex). But then the straight path could be traversed faster and still remain admissible, contradicting the assumption that T was the minimal travel time.

The formula for travel time is now clear. Since W is given by Eq. (12), the optimal path from $\boldsymbol{x}_a$ to $\boldsymbol{x}_b$ has velocity

$$w(\hat{\boldsymbol{r}}) \text{ where } \hat{\boldsymbol{r}} = \frac{\boldsymbol{x}_b - \boldsymbol{x}_a}{|\boldsymbol{x}_b - \boldsymbol{x}_a|},$$

and its travel time is

$$T(\boldsymbol{x}_a, \boldsymbol{x}_b) = \frac{|\boldsymbol{x}_b - \boldsymbol{x}_a|}{w(\hat{\boldsymbol{r}})}. \tag{14}$$

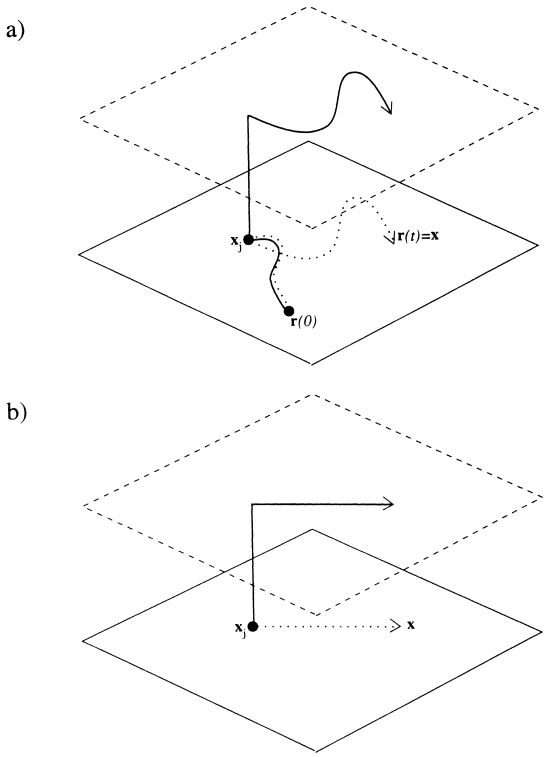

Fig. 4. (a) A non-optimal path starting in the plane of the substrate, residing for a time at the source $\boldsymbol{x}_j$, then proceeding to the surface position above the point $\boldsymbol{x}$. The dotted line shows the trajectory $\boldsymbol{r}(t)$ in Eq. (13); the solid line is the path in physical space. (b) The optimal path for Eq. (13). The solid line gives the history of the ledge that forms the surface at $\boldsymbol{x}$.

Our argument that minimal-travel-time paths are straight also shows that travel time satisfies a triangle inequality:

$$T(\boldsymbol{x}_a, \boldsymbol{x}_c) \leq T(\boldsymbol{x}_a, \boldsymbol{x}_b) + T(\boldsymbol{x}_b, \boldsymbol{x}_c). \tag{15}$$

Thus travel time behaves a lot like a metric, though it is not necessarily symmetric ($T(\boldsymbol{x}_j, \boldsymbol{x}) \neq T(\boldsymbol{x}, \boldsymbol{x}_j)$ if $U(\hat{\boldsymbol{n}}) \neq U(-\hat{\boldsymbol{n}})$).

Returning to the variational principle (13), a minor extension of the preceding arguments shows that the optimal path must start at a conveniently chosen screw dislocation site $\boldsymbol{x}_j$, reside there for time $t - T(\boldsymbol{x}_j, \boldsymbol{x})$, then proceed directly to $\boldsymbol{x}$ with velocity $w\left((\boldsymbol{x} - \boldsymbol{x}_j)/(|\boldsymbol{x} - \boldsymbol{x}_j|)\right)$. Optimization over all possible choices of $\boldsymbol{x}_j$ gives our solution formula (1). If $t < T(\boldsymbol{x}_j, \boldsymbol{x})$ for all j then there is no admissible path starting at a screw and ending at $\boldsymbol{x}$; the optimal path is indeterminate in this case, and $h(\boldsymbol{x}, t) = 0$.

Suppose the optimal path starts at $\boldsymbol{x}_j$. The associated path in physical space, visualized in Fig. 4(b), rises above $\boldsymbol{x}_j$ for time $t - T(\boldsymbol{x}_j, \boldsymbol{x})$ with velocity v_j, achieving height $h(\boldsymbol{x}, t) = v_j(t - T(\boldsymbol{x}_j, \boldsymbol{x}))$. Then it proceeds horizontally towards $\boldsymbol{x}$ during the remaining time $T(\boldsymbol{x}_j, \boldsymbol{x})$. It traces the physical history of the ledge which forms the surface of the film at location $\boldsymbol{x}$ and time t.

If there is just a single screw dislocation at the origin growing vertically with velocity v_0, our solution formula becomes $h(\boldsymbol{x}, t) = v_0 \max\{[t - T(\boldsymbol{0}, \boldsymbol{x})], 0\}$, and the region on the substrate covered by the film is a scaled copy of the Wulff shape:

$$h(\boldsymbol{x}, t) > 0 \Leftrightarrow T(\boldsymbol{0}, \boldsymbol{x}) < t \Leftrightarrow \boldsymbol{x} \in tW. \tag{16}$$

We thus recover the well-known fact that the Wulff shape expands self-similarly under the flow with normal velocity U. Notice that if $\boldsymbol{r}$ lies at the boundary of tW, $w(\boldsymbol{r}/|\boldsymbol{r}|)$ is the *radial* velocity of W; the normal velocity is $U(\hat{\boldsymbol{n}})$ where $\hat{\boldsymbol{n}}$ achieves the optimum in Eq. (12). Our analysis is restricted to convex velocities, but the Wulff shape is known to expand self-similarly even when the velocity is not convex. This can be used to show that the Wulff shape is the large-time asymptotic growth shape of any set [24].

The analysis of Frank [20] rests on the observation that the characteristics of Eq. (5) are straight lines; see also [25]. These characteristics are in fact the optimal paths for our variational principle.

3.4. Physical correctness of the solution formula

Our solution formula (1) is simple. We have linked it to a differential equation (6) and a variational principle (13). But is it physically correct?

The physical picture is this. The jth screw dislocation rises, generating new growth layers, at rate v_j. Each new growth layer spreads horizontally, continuing to spread until it gets blocked by a ledge coming from another source. It can happen that a screw dislocation gets covered by a ledge originating at another, faster-growing source; once this occurs the covered screw dislocation is inactivated, i.e. it ceases to generate new growth layers.

To validate our solution formula, we shall check its consistency with two key aspects of the physical picture:

1. The growth layer which, according to the solution formula, arrives at the surface of the film at position $\boldsymbol{x}$ and time t has not been blocked by another growth layer at an earlier time.
2. Once a source gets covered it plays no further role in the solution formula.

To clarify assertion 1, and to convince the reader that it is not entirely trivial, we begin by examining a slightly different setting where it is false. Suppose the horizontal growth velocity varies from cone to cone – isotropic, say, but with magnitude U_j for layers generated at $\boldsymbol{x}_j$. It would be tempting to propose a 'solution formula' analogous to Eq. (1), giving the film thickness $h(\boldsymbol{x}, t)$ as the envelope of the profiles of individual cones. However, such a formula would be *wrong*. To see why, consider the cross-sections of two initially non-intersecting cones at some fixed height. As time advances, these level sets eventually meet one another, blocking further growth at the associated grain boundary. However, the proposed 'solution formula' propagates the two cones independently. The cross-section with the larger normal velocity eventually passes through and completely engulfs the other one. When it has done so, the 'solution formula' puts its boundary at the surface of the film. Thus assertion 1 fails: the ledge that arrives, according to the 'solution formula', at the surface of the film at position $\boldsymbol{x}$ and time t may in fact have had its growth blocked at an earlier time.

There is nothing physically pathological about this example. The same sort of difficulty arises if individual cones grow with different anisotropies $U_j(\hat{\boldsymbol{n}})$ – as well they might, if the grains have different crystallographic orientations in the a–b plane. However, the methods of this paper are simply not appropriate for modeling the growth of multiphase systems and polycrystals. For such systems there is no solution formula or variational principle. There has been some work on simulation using level-set methods [26], and on the behavior near triple points [27–29], however, the situation is not as well understood as the single-phase case considered here.

We turn to the verification of assertion 1. Let $h(\boldsymbol{x}, t)$ be given by the solution formula (1), and consider a fixed location $\boldsymbol{x}$ and time t such that $h(\boldsymbol{x}, t) > 0$. The ledge which, according to the solution formula, arrives at the surface at $(\boldsymbol{x}, t)$ originates from source $\boldsymbol{x}_j$ such that

$$v_j[t - T(\boldsymbol{x}_j, \boldsymbol{x})] \geq v_k[t - T(\boldsymbol{x}_k, \boldsymbol{x})] \text{ for all } k. \tag{17}$$

Its history (according to the solution formula) is described by the optimal path for Eq. (13): the ledge was created at time $t - T(\boldsymbol{x}_j, \boldsymbol{x})$, when the source $\boldsymbol{x}_j$ had just reached height $v_j[t - T(\boldsymbol{x}_j, \boldsymbol{x})] = h(\boldsymbol{x}, t)$; then it propa-

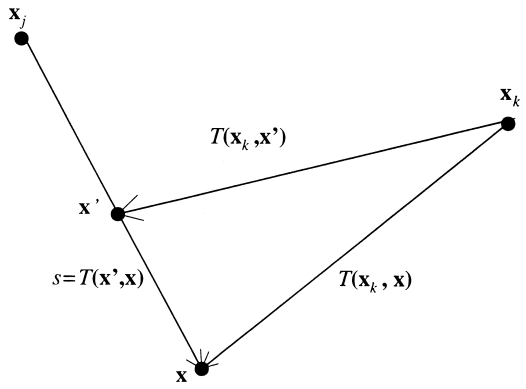

Fig. 5. Illustration of the argument validating the physical correctness of the solution formula. The points $\boldsymbol{x}_j$ and $\boldsymbol{x}_k$ are the locations of screw dislocations. The ledge arriving at location $\boldsymbol{x}$ at time t originated from the source at $\boldsymbol{x}_j$. The point $\boldsymbol{x}'$ is on the (straight) path between $\boldsymbol{x}_j$ and $\boldsymbol{x}$. The travel time from $\boldsymbol{x}'$ to $\boldsymbol{x}$ is s.

gated with constant speed to $\boldsymbol{x}$, taking time $T(\boldsymbol{x}_j, \boldsymbol{x})$ to get there. We must show that it did not get blocked on the way.

Our task is to show that from the moment this ledge was created until the moment it arrived at $\boldsymbol{x}$, the solution formula put this ledge at the surface of the film. At time $t - s$, this amounts to the assertion that

$$h(\boldsymbol{x}, t) = v_j[t - s - T(\boldsymbol{x}_j, \boldsymbol{x}')] \geq v_k[t - s - T(\boldsymbol{x}_k, \boldsymbol{x}')] \text{ for all } k, \tag{18}$$

where $\boldsymbol{x}'$ is the position of the ledge at time $t - s$, i.e. the point along the segment from $\boldsymbol{x}_j$ to $\boldsymbol{x}$ where $T(\boldsymbol{x}', \boldsymbol{x}) = s$. We must show this for $0 \leq s \leq T(\boldsymbol{x}_j, \boldsymbol{x})$. The first equality is obvious since $s + T(\boldsymbol{x}_j, \boldsymbol{x}') = T(\boldsymbol{x}_j, \boldsymbol{x})$ (see Fig. 5). The inequality is an easy consequence of Eq. (17) and

$$s + T(\boldsymbol{x}_k, \boldsymbol{x}') \geq T(\boldsymbol{x}_k, \boldsymbol{x}),$$

a special case of the triangle inequality (15).

Now let us verify assertion 2. We can use the notation of the previous paragraphs: it suffices to show that the source $\boldsymbol{x}_j$ identified by Eq. (17) was not covered prior to time $T(\boldsymbol{x}_j, \boldsymbol{x})$. This amounts to the assertion that for $t \geq s \geq T(\boldsymbol{x}_j, \boldsymbol{x})$,

$$v_j(t - s) \geq v_k[t - s - T(\boldsymbol{x}_k, \boldsymbol{x}_j)] \text{ for all } k. \tag{19}$$

We need only consider k such that $t - s - T(\boldsymbol{x}_k, \boldsymbol{x}_j) > 0$. If $v_j \geq v_k$ then

$$v_j(t - s) \geq v_j[t - s - T(\boldsymbol{x}_k, \boldsymbol{x}_j)] \geq v_k[t - s - T(\boldsymbol{x}_k, \boldsymbol{x}_j)]$$

as desired. If $v_j < v_k$, we observe that Eq. (19) holds for $s = T(\boldsymbol{x}_j, \boldsymbol{x})$, because it reduces to Eq. (18) (since $\boldsymbol{x}' = \boldsymbol{x}_j$ for this choice of s). But when $v_j < v_k$ this implies Eq. (19) holds for all $s > T(\boldsymbol{x}_j, \boldsymbol{x})$.

The thoughtful reader might have some second thoughts about the appropriateness of our assertion 2. A dislocation in a crystalline solid cannot end in the interior. So what becomes of a screw dislocation after it gets covered? The answer, we suppose, is that it continues to reach the surface of the film – but because it emerges on a narrow terrace rather than a mountain top, it cannot develop a growth spiral and so it does not nucleate new growth layers. In truth, the presence of such dislocations on the terraces could influence the horizontal velocities of ledges as they sweep across the terraces. Our model ignores this effect.

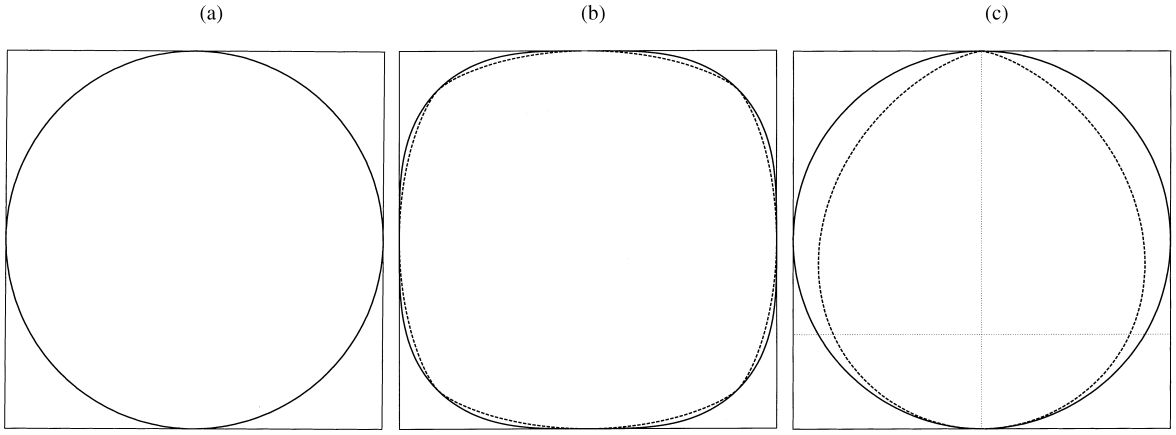

Fig. 6. Polar plots of some speed functions and the associated Wulff shapes (dashed inner regions): (a) the isotropic case $U = 1$, (b) the squarish anisotropy Eq. (20), and (c) the asymmetric anisotropy Eq. (21) (not to scale).

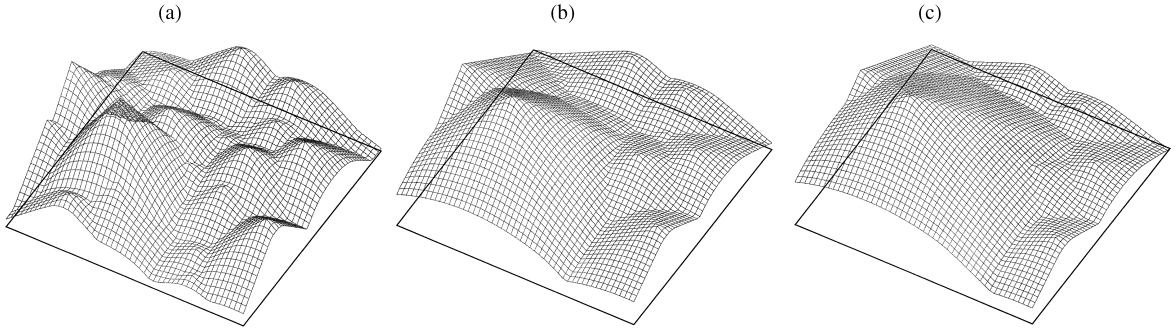

Fig. 7. Time-series of a film growing from randomly distributed sources with the anisotropic speed function (20) and heterogeneous vertical growth rates. The large cone on the left side of the figure eventually consumes all the others.

3.5. Some examples

Figs. 6(a–c) show the polar plots of three speed functions and their corresponding Wulff shapes. Fig. 6(a) describes the isotropic case $U(\hat{\boldsymbol{n}}) = 1$, for which the speed function and Wulff shape coincide; Fig. 6(b) describes the speed function

$$U(\hat{\boldsymbol{n}}) = 1 + \tfrac{1}{8}\sin^2(2\theta), \tag{20}$$

whose anisotropy is characteristic of YBCO growth (here θ is the angle that the vector $\hat{\boldsymbol{n}}$ makes with a fixed axis in the substrate plane); Fig. 6(c) describes the speed function

$$U(\hat{\boldsymbol{n}}) = \frac{1}{2 - \cos(\theta)}. \tag{21}$$

chosen to illustrate a case when the travel time is not symmetric. Convexity in the sense of Eq. (3) requires that the polar plot of $1/U$ be a convex figure in the plane, or equivalently that $U + U_{\theta\theta}$ be positive; this is the case for all three examples.

Figs. 7(a–c) gives a time series of snapshots of the surface of a film growing under the second of these three speed laws. It was obtained by evaluating the solution formula (1) for a particular choice of sources $\boldsymbol{x}_j$ and velocities v_j.

4. The case of nonuniform normal velocities

The aim of this section is to explore, in a qualitative way, the effects of variation in the horizontal growth rate $U(\hat{\boldsymbol{n}})$ from one cone to the next. Our former assumption, that the speed function $U(\hat{\boldsymbol{n}})$ is the same for the entire film, is valid when the terraces are much wider than the surface diffusion length or, equivalently, when the cones have sufficiently small slopes. When the terraces are very narrow, the normal velocity of ledges is roughly proportional to terrace width. We can connect these two limits by making the normal velocity U a function of the terrace width w. For simplicity, we restrict our discussion to the isotropic case, and we assume the relationship $U = w/(1+w)$. This choice interpolates between diffusion-limited behavior ($U = 1$) when the terraces are very wide and kinetic-limited behavior ($U \propto w$) when the terraces are very narrow.

In the continuum limit the terrace width w is inversely proportional to the surface gradient, say $w = c/|\boldsymbol{\nabla} h|$, and $U = w/(1 + w)$ becomes $U = c/(c + |\boldsymbol{\nabla} h|)$. Setting $c = 1$ by a suitable nondimensionalization, and substituting this expression for U in Eq. (6), we arrive at the evolution equation

$$h_t = \frac{|\nabla h|}{1 + |\nabla h|} + \sum_j v_j I(\boldsymbol{x} - \boldsymbol{x}_j). \tag{22}$$

We emphasize that while U is no longer constant, it is not chosen from a distribution (like the vertical growth rates v_j). Rather, it is a deterministic function of $|\nabla h|$. We choose the vertical growth rates from a distribution because they are determined by local conditions near the centers of the spirals. We treat U differently, specifying it as a function of ∇h, because it is determined by more global considerations – namely the flux of material to the surface.

An immediate consequence of Eq. (22) is the restriction of the vertical growth rates $v_j = h_t$ to the interval

$$0 \leq h_t < 1,$$

with the upper bound being approached for increasingly steep cones.

Like Eq. (6), Eq. (22) admits individual cone-shaped solutions:

$$h_j(\boldsymbol{x}, t) = v_j \left(t - \frac{|\boldsymbol{x} - \boldsymbol{x}_j|}{1 - v_j} \right), \tag{23}$$

but a superposition formula analogous to Eq. (1),

$$h(\boldsymbol{x}, t) = \max_j \left[v_j \left(t - \frac{|\boldsymbol{x} - \boldsymbol{x}_j|}{1 - v_j} \right), 0 \right], \tag{24}$$

is no longer valid. Physically, this upper-envelope type solution fails for the simple reason described in Section 3.4: a cone with a fast-expanding circular cross-extension will eventually pass through a slow-expanding cross-section, so that the computation of the solution becomes history dependent (see [14] for another example of a history-dependent film-growth model). Mathematically, this happens because the extended speed function $|\boldsymbol{\nabla} h| U(\boldsymbol{\nabla} h)$ is nonconvex (Fig. 8). This prevents us from repeating the analysis of Section 3.2 (see Eq. (11) and the discussion just after it). Therefore we no longer have the crucial triangle inequality (15) that was used to prove the validity of the solution formula (1).

One can still solve the evolution equation (22) numerically. But lacking a solution formula, one cannot expect analytical results analogous to those presented in the following section. The new formula (23) is, however, valid up to the point of overlap and near the center of any exposed spiral. From this we deduce that the vertical and horizontal growth rates are in fact related:

$$U_j = 1 - v_j.$$

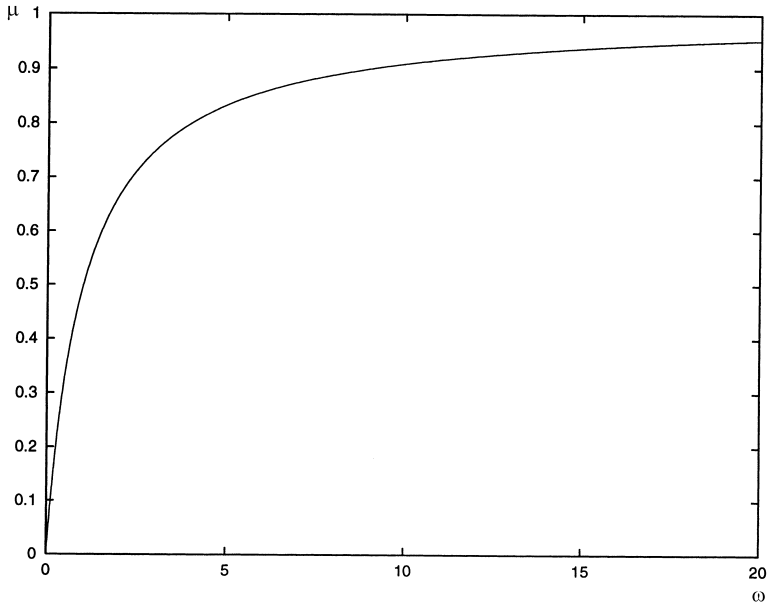

Fig. 8. Plot of the assumed relationship $U = w/(1 + w)$ between step width and normal velocity.

Thus, in analyzing the diffusion-limited regime, we are neglecting small changes in the horizontal velocity

$$U_j \sim 1 - \epsilon \tilde{U}_j,$$

but we take into account leading order variations in the vertical growth rate

$$v_j \sim \epsilon \tilde{v}_j \ll 1. \tag{25}$$

5. Analytic results for expected coarsening rates and surface roughness in the diffusion-limited growth regime

We explained in Section 2 how heterogeneity of the vertical growth rates provides a coarsening mechanism, whereby faster-growing cones overtake their slower-growing neighbors. This section determines the time-evolution of the density of uncovered spirals. We also find the statistics of surface height, leading to formulas for the evolution of mean thickness and surface roughness. First, however, we briefly discuss the case when all the vertical growth rates are equal.

5.1. Coarsening and Voronoi tesselations

Let $h_j(\boldsymbol{x}, t)$ be the profile of the cone centered at $\boldsymbol{x}_j$:

$$h_j(\boldsymbol{x}, t) = \max\{v_j[t - T(\boldsymbol{x}_j, \boldsymbol{x})], 0\}.$$

The position of the grain boundary between the cones centered at $\boldsymbol{x}_j$ and $\boldsymbol{x}_k$ is the locus of points G_{jk} where the heights of the cones are equal:

$$G_{jk} = \{\boldsymbol{x} : h_j(\boldsymbol{x}, t) = h_k(\boldsymbol{x}, t) \geq h_l(\boldsymbol{x}, t) \text{ for all } l\}.$$

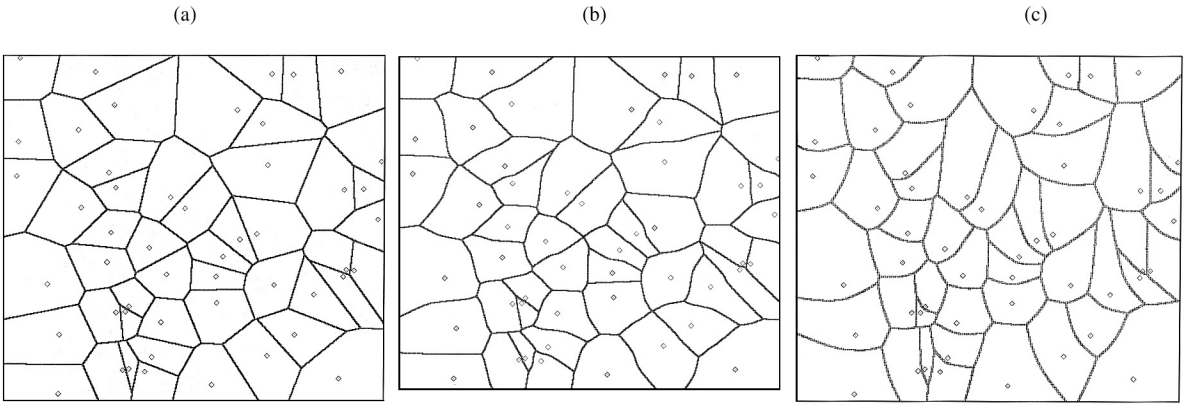

Fig. 9. Grain boundaries for the tesselations formed when all of the vertical growth rates are equal. The three cases (a–c) correspond with the speed functions plotted in Figs. 6(a–c). Source locations, indicated by diamonds, are the same for all three figures.

If the vertical velocities are all equal then the grain boundaries are stationary, i.e. they do not depend on t. If in addition U is isotropic then G_{jk} lies along the line equidistant from $\boldsymbol{x}_j$ and $\boldsymbol{x}_k$. The grain boundaries are the polygons formed by these lines; each point in the plane is assigned to the nearest nodal point. The resulting grain structure, known as a Voronoi tessellation, and is a familiar concept in the literature on crystal growth [30]. Figure 9(a) gives an example of a Voronoi tesselation. If U is anisotropic and the vertical velocities are all equal, the grain structure is still a static tesselation: each point $\boldsymbol{x}$ is assigned to the node with the shortest travel time $T(\boldsymbol{x}_j, \boldsymbol{x})$. Figures 9(b,c) give examples of such tesselations; note that the grain boundaries are no longer straight in this case.

When the vertical velocities are heterogeneous, faster-growing cones encroach upon their slow-growing neighbors. If there is a maximal velocity and a nonzero density of sources with maximal velocity, then the asymptotic growth state is the Voronoi tesselation formed by the fastest growing cones. However, for an infinite system with a continuous distribution of growth rates, coarsening continues indefinitely.

5.2. *Formulas for the spiral density and surface statistics*

We now examine the statistical properties of the growing film. Our analysis assumes that the sources are distributed as a Poisson point process. It capitalizes on the special properties of Poisson processes [31], and is closely analogous to the work of Molchanov et al. [15].

Let the initial density of nucleation sites be λ_0. We seek a formula for the expected density of uncovered sites at later times, $\lambda(t)$. Clearly $\lambda(t)$ is the product of the initial density times the probability that an arbitrary site $\boldsymbol{x}_j$ remains uncovered. The condition that $\boldsymbol{x}_j$ remain uncovered at time t is

$$tv_j > v_k(t - T(\boldsymbol{x}_k, \boldsymbol{x}_j)), \quad \text{for all } k \neq j.$$

We simplify the notation by taking the origin to be at $\boldsymbol{x}_j$ and removing the subscript on v_j:

$$tv > v_k(t - T(\boldsymbol{x}_k, \boldsymbol{0})). \tag{26}$$

Let $F(v)$ be the probability that an arbitrary spiral has a growth rate less than or equal to v – i.e. the cumulative distribution function (CDF) for the vertical growth rates. The probability P_k that Eq. (26) is satisfied for a given k is

$$P_k = \begin{cases} 1, & T(\boldsymbol{x}_k, \boldsymbol{0}) \geq t \\ F\left(tv/(t - T(\boldsymbol{x}_k, \boldsymbol{0}))\right), & T(\boldsymbol{x}_k, \boldsymbol{0}) < t. \end{cases}$$

The probability $P(t)$ that Eq. (26) is satisfied for all k at time t is the expected value of the product of the P_k's:

$$P(t) = \left\langle \prod_k P_k(\boldsymbol{x}_k, v, t) \right\rangle = \left\langle \exp\left[\sum_k \log P_k \right] \right\rangle,$$

where the brackets indicate an average over $v > 0$ and all possible configurations of the PPP.

The average over the $\boldsymbol{x}_k$ can be evaluated in terms of an integral using Campbell's theorem (see [31]):

$$P(t) = \left\langle \exp\left[\lambda_0 \int_{T(\boldsymbol{x},\boldsymbol{0})<\infty} (P(\boldsymbol{x}, v, t) - 1)\ \mathrm{d}\boldsymbol{x} \right] \right\rangle_v = \left\langle \exp\left[-\lambda_0 t^2 \int_{T(\boldsymbol{x},\boldsymbol{0})<1} \tilde{F}\left(\frac{v}{1 - T(\boldsymbol{x}, \boldsymbol{0})} \right) \mathrm{d}\boldsymbol{x} \right] \right\rangle_v,$$

where $\tilde{F} = 1 - F$ is the complement of F and we have made the change of variables $\boldsymbol{x} \to t\boldsymbol{x}$ in the second integral. Averaging over v gives

$$\lambda(t) = \lambda_0 P(t) = \lambda_0 \int_0^\infty \exp\left[-\lambda_0 t^2 \int_{T(\boldsymbol{x},\boldsymbol{0})<1} \tilde{F}\left(\frac{v}{1 - T(\boldsymbol{x}, \boldsymbol{0})} \right) \mathrm{d}\boldsymbol{x} \right] F'(v)\, \mathrm{d}v. \tag{27}$$

Finally, making the change of variable $R = r/w(\hat{\boldsymbol{r}})$, we can write Eq. (27) in terms of the area of the Wulff shape:

$$\lambda(t) = \lambda_0 \int_0^\infty \exp\left[-2A_w \lambda_0 t^2 \int_0^1 \tilde{F}\left(\frac{v}{1 - R} \right) R\, \mathrm{d}R \right] F'(v)\, \mathrm{d}v, \tag{28}$$

where

$$A_w = \frac{1}{2} \int_0^{2\pi} w^2(\theta)\, \mathrm{d}\theta.$$

We turn now to the statistics of the surface height. Let $H(h)$ be the probability that an arbitrarily chosen point $\boldsymbol{x}'$ will have a height $h' \le h$ – in other words, the CDF for surface height. If H_j represents this probability for each cone individually, we have

$$H(h) = \left\langle \prod_{j=1}^\infty H_j(h) \right\rangle.$$

Taking $\boldsymbol{x}'$ to be at the origin, we require

$$v_j \left(t - T(\boldsymbol{x}_j, \boldsymbol{0}) \right) \le h \ \text{ for all } \ j.$$

Relating this to the CDF for the growth rates then gives

$$H_j = F\left(\frac{h}{t - T(\boldsymbol{x}_j, \boldsymbol{0})} \right),$$

and applying Campbell's theorem as before we arrive at

$$H(h; t) = \exp\left[-2A_w \lambda_0 t^2 \int_0^1 \tilde{F}\left(\frac{h/t}{1 - R} \right) R\, \mathrm{d}R \right]. \tag{29}$$

The preceding result determines, in particular, the average height and the surface roughness (standard deviation). In fact, the average height at time t is

$$\langle h(t) \rangle = \int_0^\infty h H'(h)\, \mathrm{d}h \tag{30}$$

and the surface roughness at time t is

$$\sigma_h(t) = \sqrt{\langle h^2\rangle - \langle h\rangle^2} = \left(\int_0^\infty [h^2 - \langle h\rangle^2] H'(h)\,\mathrm{d}h\right)^{1/2}. \tag{31}$$

5.3. Large-time behavior

The large-time behavior is dominated by the tail of the vertical velocity distribution, i.e. the statistics of the cones with the largest growth rates. In this section we derive the large-time asymptotic behavior for the spiral density and surface height.

We begin by writing Eq. (28) as a Laplace type integral:

$$\lambda(t) = \lambda_0 \int_0^\infty \exp[-2\,A_w \lambda_0 t^2 K(v)] F'(v)\,\mathrm{d}v, \tag{32}$$

where

$$K(v) = \int_0^1 \tilde{F}\left(\frac{v}{1-R}\right) R\,\mathrm{d}R. \tag{33}$$

Laplace's method (see e.g. Section 6.4 of [32]) shows that the large time behavior of Eq. (32) is determined by the behavior of $K(v)$ near its minimum within the range of integration. Examination of Eq. (33) reveals that this minimum is zero and it occurs in the limit $v \to \infty$. We map this minimum to the origin using the change of variable $X = \tilde{F}(v)$:

$$\lambda(t) = \lambda_0 \int_0^1 \exp[-2A_w \lambda_0 t^2 K(X)]\,\mathrm{d}X.$$

The expansion of $K(X)$ depends on the choice of growth rate distribution. As explained in Section 4 (see especially Eq. (25)), an appropriate distribution in the surface-diffusion limited case will have all $v_j \sim \mathrm{O}(\epsilon) \ll 1$. Here we use the rescaled growth rates $\tilde{v}_j \sim \mathrm{O}(1)$, so we can consider distributions which are conveniently defined for all positive values in the limit $\epsilon \to 0$:

$$\tilde{F}(\tilde{v}) = \frac{1}{\epsilon} F(v).$$

In doing so, we recognize that any realistic distribution will be *heavily* weighted to favor small growth rates. More specifically, one expects a realistic distribution to approach zero as $\tilde{v}$ approaches both zero and infinity, with most of the growth rates close to a small mean value.

We have no specific model for this distribution nor even its tail. To briefly illustrate the manner in which Eq. (32) can be used to obtain power laws for coarsening and other mesoscopic surface quantities, we use a class of Weibull distributions as an example:

$$\tilde{F}'(\tilde{v}) = \frac{\alpha}{\beta^\alpha} \tilde{v}^{\alpha-1} \mathrm{e}^{-(\tilde{v}/\beta)^\alpha}. \tag{34}$$

The large-$\tilde{v}$/small-X behavior of $K(X)$ is given by the asymptotic expansion of the integral equation (33) in the limit $R \to 0$. This expansion is relatively straightforward, being given by Watson's lemma (see [32]) after a suitable change of variables:

$$K(X) \sim X\left(\frac{1}{\alpha^2(-\log X)^2} + \mathrm{O}\left(\frac{1}{(-\log X)^3}\right)\right).$$

The integral equation (32) can be converted to a more conventional Laplace-type integral by changing variable to $Y = X\log^{-2}X$:

$$\lambda(t) \sim \lambda_0 \int_0^\delta \exp\left[-\frac{A_w}{2\lambda_0 t^2 Y}\right] \log^2 Y \, \mathrm{d}Y,$$

for any positive δ. A further change of variable to $Z = 2A_w\lambda_0 t^2 Y$ reduces the integrand to a function that can be expanded for large values of t to give known integrals. The leading order term in this expansion is

$$\lambda(t) \sim \frac{2\alpha^2}{A_w t^2}\log^2 t. \tag{35}$$

This, in turn, implies a nearly linear increase in the average grain size $1/\sqrt{\lambda(t)}$.

A similar procedure can be applied to Eq. (30). We omit the details, giving just the result:

$$\langle h(t)\rangle \sim 2^{1/\alpha}\beta t \log^{1/\alpha} t. \tag{36}$$

Thus the mean growth of the film is slightly superlinear. It would be exactly linear if the velocities v_j were all equal and there were no coarsening. The logarithmic factor reflects the gradual coarsening associated with the exponentially-decaying tail of the distribution.

We emphasize the contrast between Eqs. (35) and (36). Heterogeneity of the vertical growth rates has only a minor qualitative effect on the overall growth rate: it changes the law from linear to linear times a power of $\log t$ (Eq. (36)). However, it has a dramatic effect on the coarsening behavior: it changes the law from one of no coarsening to one with approximately linear increase in the average grain size (Eq. (35)).

It is more difficult to obtain the asymptotic behavior of the surface roughness $\sigma(t)$. One can proceed as above, but the first two terms in the expansions of $\langle h^2\rangle$ and $\langle h\rangle^2$ cancel. This suggests that the growth of the standard deviation is slightly sublinear; our simulations support this conclusion. Note that the surface roughness, like the grain-size, would not change at all if all of the vertical growth rates were the same.

Finally, it should be understood that this model is in no way limited to exponentially decaying distributions. If subsequent theory or experiment should suggest otherwise, it is a simple matter to reevaluate the large-time asymptotic behavior of Eq. (32).

5.4. Discrete distributions

The integrals in Eqs. (28) and (29) are easy to evaluate when the distribution of growth rates is discrete. Suppose the possible growth rates are $0 < V_1 < V_2 < \ldots < V_N$, with $P(v_j = V_n) = p_n$ and $\sum_{n=1}^N p_n = 1$. For notational convenience we set $V_0 = 0$, $p_0 = 0$, and $V_{N+1} = \infty$. The CDF of this discrete probability distribution is

$$F(v) = F_n = \sum_{k=0}^{n} p_k \quad \text{when} \quad V_n \le v < V_{n+1}.$$

Its complement is $\tilde{F}_n = 1 - F_n$ when $V_n \le v < V_{n+1}$.

Our expression (28) for the uncovered spiral density evaluates to

$$\lambda(t) = \lambda_0 \sum_{n=1}^{N} p_n \exp\left[-A_w\lambda_0 t^2 \sum_{k=n}^{N-1} \tilde{F}_k \cdot (R_{k+1}^2 - R_k^2)\right],$$

where

$$R_k = 1 - \frac{V_n}{V_k},$$

and the inner sum is understood to be zero if $n > N-1$. Notice that the last term in the outer sum is just $\lambda_0 p_N$ and the other terms decay exponentially in time. The asymptotic uncovered spiral density is just the fraction of the original spirals that grow at the fastest rate, as expected.

Our expression (29) for the distribution of surface heights becomes

$$H(h;t) = \exp\left[-A_w \lambda_0 t^2 \sum_{k=n}^{N-1} \tilde{F}_k \cdot (R_{k+1}^2 - R_k^2)\right], \tag{37}$$

when $tV_{n-1} \le h < tV_n$, with the notation

$$R_k = 1 - \frac{h}{tV_k}.$$

The expressions for average height and surface roughness are most conveniently evaluated numerically. This is best done by first integrating by parts to eliminate the derivative of Eq. (37).

The growth associated with any continuous distribution can be approximated by using a suitable discrete distribution. This amounts to approximating the integrals in Eqs. (28) and (29) by Riemann sums.

6. Simulations

The analytic results of the previous section are useful for examining simple cases and large-time asymptotics. Other results such as transient behavior are best obtained by evaluating the integrals in Eqs. (28) and (29) numerically, or else evaluating the solution formula (1) directly using a large number of randomly generated sources. Figs. 10(a–c) compare typical results from simulations done both ways.

We have thus far ignored any variation in the nucleation times of the spirals. The experiments of Yeadon et al. [10] suggest that such variation can be important. It can be included by making a minor change in our solution formula:

$$h(\boldsymbol{x}, t) = \max_j [v_j(t - t_j - T(\boldsymbol{x}_j, \boldsymbol{x})), 0]. \tag{38}$$

Here t_j represents the nucleation time of the jth source; it should be drawn (like v_j) from a specified probability distribution. Figure 11 shows the result of including this effect, using a Weibull distribution for t_j. Nucleation competes with coarsening: the density of spirals increases initially (dominated by nucleation) then decreases (dominated by coarsening). The competition between these two effects can be adjusted by tuning the parameter β in the Weibull distribution for t_j. To generate Fig. 11 we chose this parameter to make the result resemble the experimental data of Yeadon et al. [10].

One could, in principle, use Eq. (22) to collect statistics for the non-diffusion-limited case. We have not done this because it requires a huge calculation: one would have to step through the entire history of the film's evolution, with large enough sample sizes to keep a statistically significant number of grains. Such a calculation would be of interest; alternatively one might hope for further analytical progress that would simplify the task.

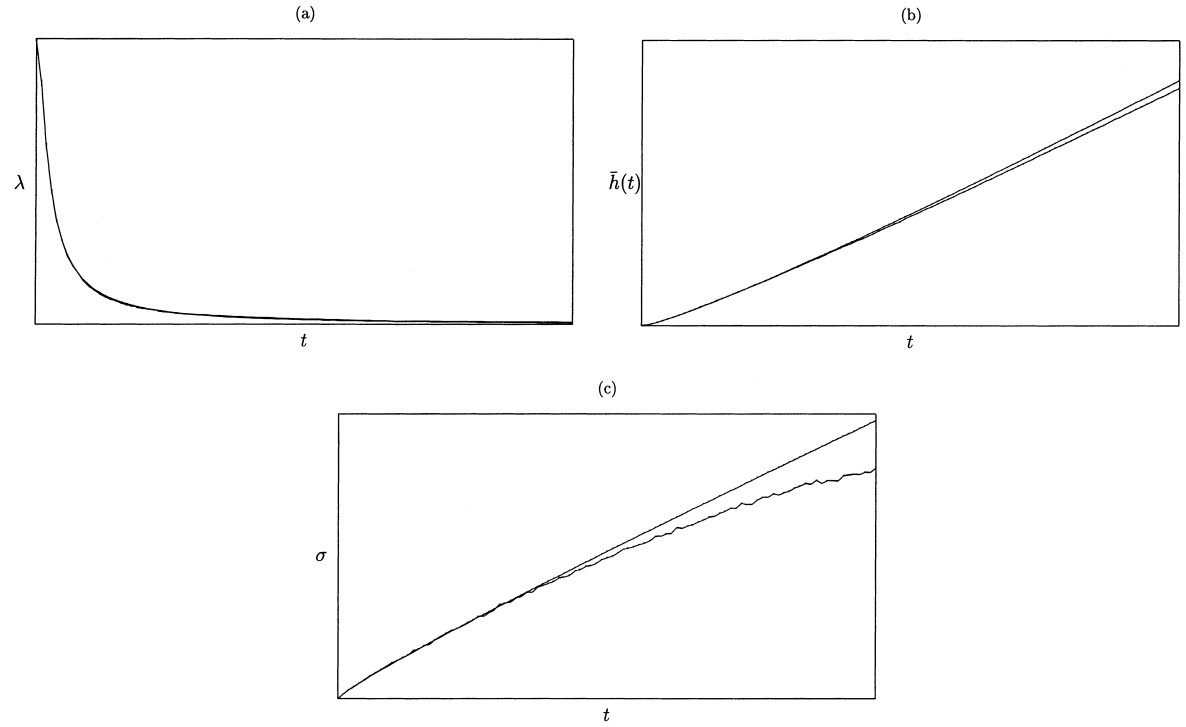

Fig. 10. Comparison of analytic predictions and the results of simulations for (a) uncovered spiral density, (b) mean surface height, and (c) surface roughness (standard deviation of surface height).

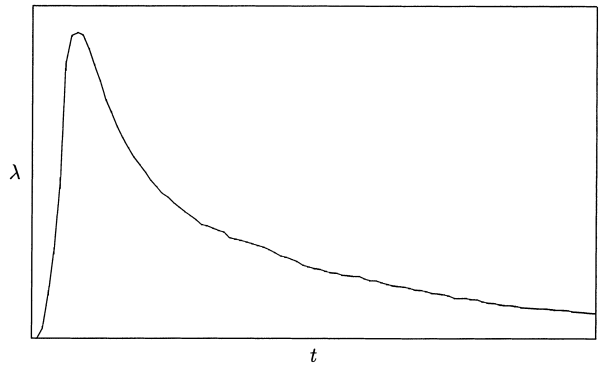

Fig. 11. Uncovered spiral density as a function of time using the generalized solution formula (38), which distributes the nucleation times. The resulting graph is qualitatively similar to the experimental results of Yeadon et al. [10].

7. Conclusions

We have explained how heterogeneity of the vertical growth rates can lead to coarsening in spiral-mode growth. The mechanism is a sort of geometrical competition, whereby faster-growing spirals outgrow their neighbors. Under the frequently reasonable assumption of diffusion-limited growth, our model permits explicit numerical evaluation of statistical features such as the density of uncovered spirals, the overall growth rate, and the surface roughness. The predictions of our model are not ‘universal’. Rather, they depend on constitutive information – namely, the

distribution of vertical growth rates. The large-time asymptotics depend only on the tail of this distribution, which may be obtainable from an as yet undeveloped theory or from empirical evidence.

Other plausible explanations have been offered for the coarsening observed in YBCO thin films. Yeadon et al. [10] suggest a mechanism based on the motion of screw dislocations under elastic stress, but a quantitative model based on this idea has yet to be developed. Ortiz et al. [12] suggest a mechanism based on a tendency to decrease the defect energy of valleys (grain boundaries) at the surface of the film. Their model is very quantitative, with no tunable parameters, and it predicts that grain size should scale like $t^{1/3}$ as $t \to \infty$. This scaling law seems consistent with some of the (very limited) experimental data that is available, but disagrees with results obtained by Blank et al. [11] that suggest a $t^{1/2}$ time-dependence. Our results using the example of Wiebull statistics suggest a linear growth in the grain size for large times, but this is, of course, dependent on the choice of vertical growth-rate distribution. Distributions with tails that decay more slowly are apt to yield slower coarsening rates. It is not clear, however, whether the existing data on coarsening of YBCO represents an asymptotic large-time regime or simply some intermediate-time transient.

One motivation for studying film microstructure is the hope that it can be influenced by variation in growth conditions. To this end it would be natural to couple our growth model with a description of the deposition process, for example vapor deposition. Coupling of this type has recently been considered in a related setting [33]. To couple our growth model with a vapor deposition flow model, the horizontal growth rate $U(\hat{\boldsymbol{n}})$ and the vertical growth rates v_j should depend in some way on supersaturation. Also, the fluid-film boundary condition should reflect the overall growth rate. Notice that this growth rate is transient even when the supersaturation is constant, as a consequence of coarsening. The implementation of such coupling remains a task for the future.

Acknowledgements

This work was funded by NSF and DARPA through the project Virtual Integrated Processing of YBCO Thin Films. We are grateful to Weinan E. and Michael Ortiz for many helpful discussions.

References

[1] A.A. Chernov, Formation of crystals in solutions, Cont. Phys. 30 (1989) 251–276.
[2] W.K. Burton, N. Cabrera, F.C. Frank, The growth of crystals and the equilibrium structure of their surfaces, Phil. Trans. R. Soc. London 243A (1951) 299–358.
[3] N. Cabrera, M.M. Levine, On the dislocation theory of evaporation of crystals, Phil. Mag. 1 (1956) 450–458.
[4] H. Müller-Krumbhaar, T.W. Burkhardt, D.M. Kroll, Generalized kinetic equation for crystal growth, J. Cryst. Growth 38 (1977) 13–22.
[5] R.H. Swendsen, P.J. Kortman, D.P. Landau, H. Müller-Krumbhaar, Spiral growth of crystals: simulations on a stochastic model, J. Cryst. Growth 35 (1976) 73–78.
[6] R. Xiao, J.I.D. Alexander, F. Rosenberger, Growth morphologies of crystal surfaces, Phys. Rev. A 43 (1991) 2976–2992.
[7] I.S. Aranson, A.R. Bishop, I. Daruka, V.M. Vinokur, Ginzburg–Landau theory of spiral surface growth, Phys. Rev. Lett. 80 (1998) 1770–1773.
[8] A. Karma, M. Plapp, Spiral surface growth without desorption, Phys Rev. Lett. 81 (1998) 4444–4447.
[9] I.D. Raistrick, M. Hawley, Scanning tunneling and atomic force microscope studies of thin sputtered films of $YBa_2Cu_3O_{7-\delta}$, in: S.L. Shindé, D.A. Rudman (Eds.), Interfaces in High-T_c Superconducting Systems, Springer, New York, 1994, pp. 28–70.
[10] M. Yeadon, M. Aindow, F. Wellhöfer, J.S. Abell, Topographical development and misfit relief in laser-ablated heteroepitaxial $YBa_2Cu_3O_{7-\delta}$ thin films, J. Cryst. Growth 172 (1997) 145–155.
[11] D.H.A. Blank, M.E. Bijlsma, R. Moerman, H. Rogalla, F.J.B. Stork, A. Roshko, Surface roughness and height–height correlations dependence on thickness of YBaCuO thin films, J. Alloys Compounds 251 (1997) 31–33.
[12] M. Ortiz, E. Repetto, H. Si, A continuum model of kinetic roughening and coarsening in thin films, J. Mech. Phys. Solids (1998), submitted for publication.
[13] C. Tang, S. Alexander, R. Bruinsma, Scaling theory for the growth of amorphous films, Phys. Rev. Let. 64 (1990) 772–775.

[14] J.M. Thijssen, H.J.F. Knops, A.J. Dammers, Dynamic scaling in polycrystalline growth, Phys. Rev. B 45 (1992) 8650–8656.
[15] S.A. Molchanov, D. Surgailis, A. Woyczynski, The large-scale structure of the universe and quasi-Voronoi tessellation of shock fronts in forced Burgers turbulence in $\boldsymbol{R}^{\boldsymbol{d}}$, Ann. Appl. Prob. 7 (1997) 200–228.
[16] S.J. Pennycook, M.F. Chisholm, D.E. Jesson, R. Feenstra, S. Zhu, X.Y. Zheng, D.J. Lowndes, Growth and relaxation mechanisms of $YBa_2Cu_3O_{7-x}$ films, Physica C 202 (1992) 1–11.
[17] D.G. Schlom, D. Anselmetti, J.G. Bednorz, Ch. Gerber, J. Mannhart, Epitaxial growth of cuprate superconductors from the gas phase, J. Cryst. Growth 137 (1994) 259–267.
[18] S. Osher, J.A. Sethian, Fronts propagating with curvature-dependent speed: algorithms based on Hamilton–Jacobi formulation, J. Comp. Phys. 79 (1988) 12–49.
[19] J.A. Sethian, Level Set Methods, Cambridge University Press, Cambridge, 1996.
[20] F.C. Frank, On the kinematic theory of crystal growth and dissolution processes, in: R.H. Doremus (Ed.), Growth and Perfection of Crystals, Chapman & Hall, London, 1958, pp. 411–419.
[21] J.W. Cahn, J.E. Taylor, C. Handwerker, Evolving crystal forms: Frank's characteristics revisited, in: R.G. Chambers, J.E. Enderby, A. Keller, A.R. Lang, J.W. Steeds (Eds.), Sir Charles Frank, OBE, FRS, An Eightieth Birthday Tribute, Hilger, New York, 1991, pp. 88–118.
[22] L.C. Evans, Partial Differential Equations, American Mathematical Society, Providence, RI, 1998.
[23] I. Fonseca, The Wulff theorem revisited, Proc. R. Soc. London, Ser. A 432 (1991) 125–145.
[24] P. Soravia, Generalized motion of a front propagating along its normal direction: a differential games approach, Nonlinear Anal., Theory, Methods & Applns. 22 (1994) 1247–1262.
[25] J.E. Taylor, J.W. Cahn, C.A. Handwerker, Geometric models of crystal growth, Acta Metall. Mater. 40 (1992) 1443–1474.
[26] H.-K. Zhao, T. Chan, B. Merriman, S. Osher, A variational level set approach to multiphase motion, J. Comp. Phys. 127 (1996) 179–195.
[27] J.E. Taylor, The motion of multiple-phase junctions under prescribed phase-boundary velocities, J. Diff. Eqns. 119 (1995) 109–136.
[28] J.E. Taylor, A variational approach to crystalline triple junction motion, J. Stat. Phys. (1999), in press.
[29] F. Reitich, H.M. Soner, Three-phase boundary motions under constant velocities I: The vanishing viscosity method, Proc. R. Soc. Edinburgh 126A (1996) 837–865.
[30] J. Moller, Lectures on random Voronoi tessellations, in: Lecture Notes in Statistics, vol. 87, Springer, New York, 1994.
[31] J.F.C. Kingman, Poisson Processes, Oxford University Press, Oxford, 1993.
[32] C.M. Bender, S.A. Orszag, Advanced Mathematical Methods for Scientists and Engineers, McGraw-Hill, New York, 1978.
[33] S.T. Rodgers, K.F. Jensen, Multiscale modeling of chemical vapor deposition, J. Appl. Phys. 83 (1998) 524–530.